Iterative α-(de)Blending: a Minimalist Deterministic Diffusion Model

ERIC HEITZ, Unity Technologies, France
LAURENT BELCOUR, Intel Corporation, France
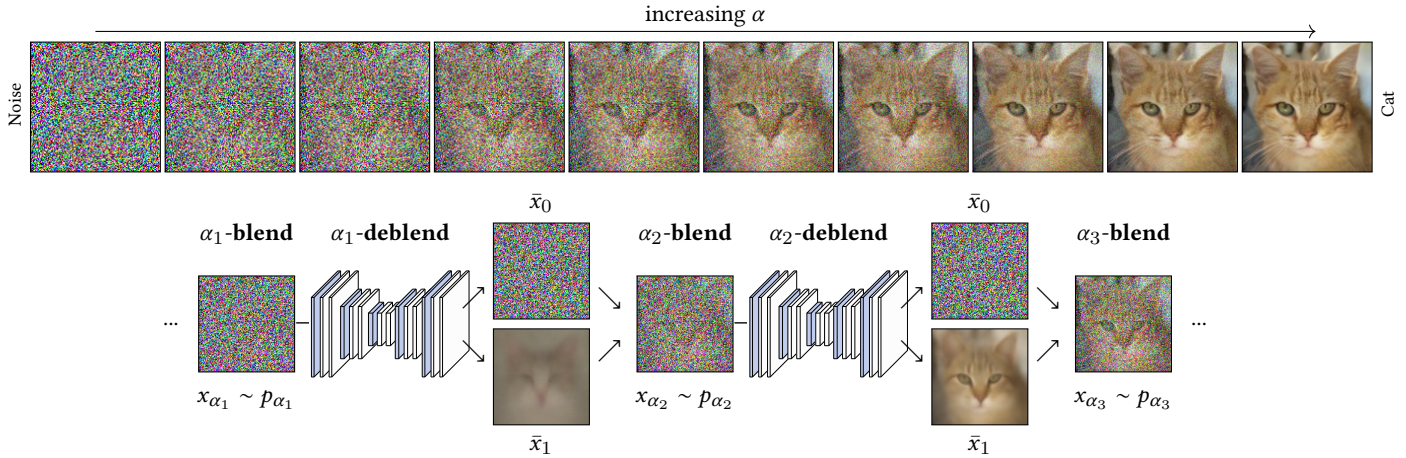THOMAS CHAMBON, Unity Technologies, France

arXiv:2305.03486v1 [cs.GR] 5 May 2023

Fig. 1. **Iterative α-blending and deblending.** In this example, we map Gaussian noise to cat images. We use a neural network trained to deblend blended Gaussian noise and cats. By deblending and reblending iteratively, we obtain a mapping between the Gaussian and cat densities.

ABSTRACT

We derive a minimalist but powerful deterministic denoising-diffusion model. While denoising diffusion has shown great success in many domains, its underlying theory remains largely inaccessible to non-expert users. Indeed, an understanding of graduate-level concepts such as Langevin dynamics or score matching appears to be required to grasp how it works. We propose an alternative approach that requires no more than undergrad calculus and probability. We consider two densities and observe what happens when random samples from these densities are blended (linearly interpolated). We show that iteratively blending and deblending samples produces random paths between the two densities that converge toward a deterministic mapping. This mapping can be evaluated with a neural network trained to deblend samples. We obtain a model that behaves like deterministic denoising diffusion: it iteratively maps samples from one density (e.g., Gaussian noise) to another (e.g., cat images). However, compared to the state-of-the-art alternative, our model is simpler to derive, simpler to implement, more numerically stable, achieves higher quality results in our experiments, and has interesting connections to computer graphics.

Additional Key Words and Phrases: diffusion models, sampling, mapping

1 INTRODUCTION

Diffusion models have recently become one of the most popular generative modeling tools [Ramesh et al. 2022]. They have outperformed state-of-the-art GANs [Karras et al. 2021, 2020] and been applied to many applications, such as image generation [Dhariwal and Nichol 2021; Rombach et al. 2021], image processing [Kawar et al. 2022; Saharia et al. 2021; Whang et al. 2022], text-to-image [Saharia et al. 2022b], video [Ho et al. 2022] or audio [Kong et al. 2020].

First, there were stochastic diffusion models... These diffusion models can all be formulated as *Stochastic Differential Equations* (SDEs) [Song et al. 2021b] such as *Langevin dynamics*. Langevin's equation models a random walk that obeys a balance between two operations related to Gaussian noise: increasing noise by adding more noise, and decreasing noise by climbing the gradient of the log density. Increasing noise performs large steps but pushes the samples away from the true density. Decreasing noise projects the samples back onto the true density. Carefully tracking and controlling this balance allows one to perform efficient random walks and provides a sampling procedure for the true density. This is the core of denoising diffusion approaches. Noise Conditional Score Networks (NCSNs) [Song and Ermon 2019, 2020] use Langevin's equation directly by leveraging the fact that the score (the gradient of the log density in Langevin's equation) can be learnt via a denoiser when the samples are corrupted with Gaussian noise [Vincent 2011]. Denoising Diffusion Probabilistic Models (DDPMs) [Ho et al. 2020; Nichol and Dhariwal 2021] use a Markov chain formalism with a Gaussian prior that provides an SDE similar to Langevin dynamics, where the score is also implicitly learnt with a denoiser.

...then came deterministic diffusion models. Langevin's SDEs variants describe an equilibrium between noise injection and noise removal. Nullifying the noise injection in these SDEs yields *Ordinary Differential Equations* (ODEs), also called *Probability Flow ODEs* [Song et al. 2021b], that simply describe the deterministic trajectory of a noisy sample projected back onto the true density. For instance, Denoising Diffusion Implicit Models (DDIMs) [Song et al. 2021a] are the ODE variants of DDPMs. These ODEs provide a smooth, deterministic mapping between the Gaussian noise density and the true density. Deterministic diffusion models have recently been proposed because an ODE requires far fewer solver iterations than its SDE counterpart. Furthermore, a deterministic mapping presents multiple practical advantages because samples are uniquely determined by their prior Gaussian noise. For instance, they can be edited or interpolated via the Gaussian noise.

Is there a simpler approach to deterministic diffusion? The point of the above story is that, in the recent line of work on diffusion models, stochastic diffusion models came *first* and deterministic diffusion models came *after*, framed as special cases of the stochastic ones. Hence they inherited the underlying mindset and mathematical framework. As a result, knowledge of advanced concepts such as Langevin dynamics, score matching, how they relate to Gaussian noise, etc., appears to be required to understand recent deterministic diffusion models. We argue that this is an unnecessary detour for something that can be framed in a much simpler and more general way. We propose a fresh take on deterministic diffusion with another mindset, using only basic sampling concepts.

- **Simpler derivation.** We derive a deterministic, diffusion-like model based on the sampling interpretation of blending and deblending. We call it Iterative α-(de)Blending (IADB) in reference to the computer graphics α-blending technique that composes images with a transparency parameter [Porter and Duff 1984]. Our model defines a mapping between arbitrary densities (of finite variance).

- **Practical improvements.** We show that, when the initial density is Gaussian, the mappings defined by IADB are exactly the same as the ones defined by DDIM [Song et al. 2021a], but with several benefits. First, our derivation leads to a more numerically stable sampling formulation. Second, our experiments show that IADB consistently outperforms DDIM in terms of final FID scores for several datasets and is more stable for a small number of sampling steps.

- **Theoretical improvements.** A side effect of our derivation is that, in contrast to DDIM, IADB does not require the assumption that the initial density is Gaussian, which is a significant generalization. Furthermore, our derivation leads to a stochastic mapping algorithm that is reminiscent of computer graphics applications.

2 BLENDING AND DEBLENDING AS SAMPLING

Initial densities. We consider two densities $p_0, p_1 : \mathbb{R}^d \to \mathbb{R}^+$ represented, respectively, by the red triangle and the green square in Figure 2. We denote their corresponding samples as $x_0 \sim p_0$ and $x_1 \sim p_1$. For independent samples x_0 and x_1, we use the notation $(x_0, x_1) \sim p_0 \times p_1$.
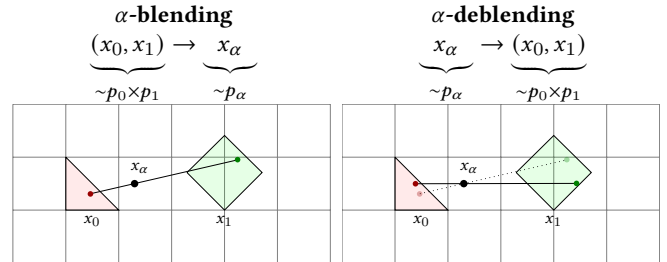

Fig. 2. **Blending and deblending as sampling operations.**

Definition of α-blending. We use p_α to refer to the density of the blended samples $x_\alpha = (1 - \alpha) x_0 + \alpha x_1$ obtained by blending random samples $(x_0, x_1) \sim p_0 \times p_1$ with a parameter $\alpha \in [0, 1]$.

Definition of α-deblending. We call the inverse sampling operation α-deblending, i.e., generating random x_0 and x_1 from the initial densities that could have been α-blended to a point x_α. Formally, it means sampling random *posteriors* $(x_0, x_1)_{|(x_\alpha, \alpha)} \sim (p_0 \times p_1)_{|(x_\alpha, \alpha)}$. The key property is that if $x_\alpha \in \mathbb{R}^d$ is a **fixed** point, the posterior densities *are not* the initial densities $p_0 \times p_1$. However, if $x_\alpha \sim p_\alpha$ is a **random** sample, the posterior densities *are* the initial densities. This follows directly from the *law of total probability* illustrated in Figure 3. In other words, α-deblending a random sample $x_\alpha \sim p_\alpha$ is equivalent to sampling $(x_0, x_1) \sim p_0 \times p_1$.
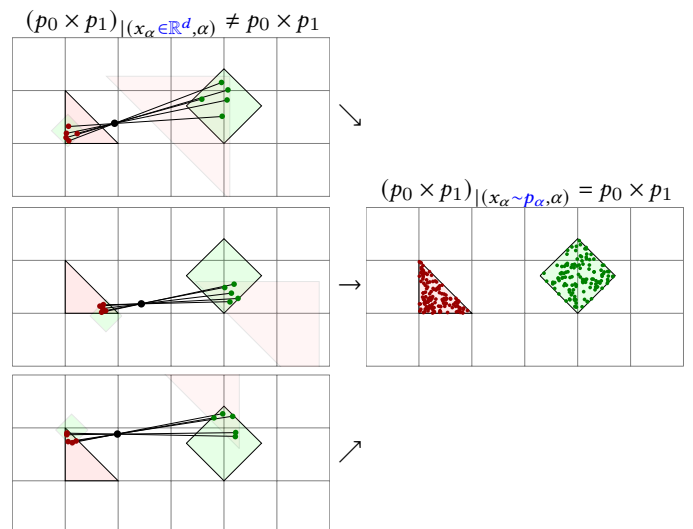

Fig. 3. **The law of total probability.** Intuitively, deblending a **fixed** $x_\alpha \in \mathbb{R}^d$ means sampling only in a subset of the initial densities. However, if $x_\alpha \sim p_\alpha$ is **random**, all these subsets are merged and the sampling occurs in the initial densities as if we had directly sampled $(x_0, x_1) \sim p_0 \times p_1$.

Definition of α-(de)blending. Let's consider two blending parameters $\alpha_1, \alpha_2 \in [0, 1]$. Using the previous proposition, we can chain α_1-deblending and α_2-blending to map a random sample $x_{\alpha_1} \sim p_{\alpha_1}$ to a random sample $x_{\alpha_2} \sim p_{\alpha_2}$. Indeed, by sampling posteriors for a random sample $x_{\alpha_1} \sim p_{\alpha_1}$, we obtain random samples $(x_0, x_1) \sim (p_0 \times p_1)$ from the initial densities, and blending them with parameter α_2 provides a random sample $x_{\alpha_2} \sim p_{\alpha_2}$. This is illustrated in Figure 4.
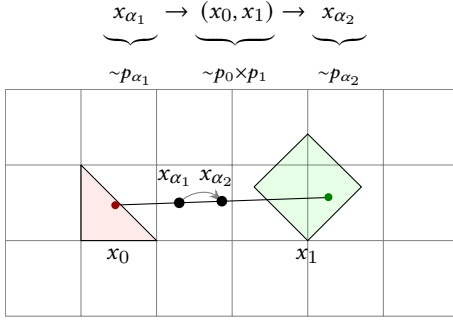

Fig. 4. α-**(de)blending.**

3 ITERATIVE α-(DE)BLENDING (IADB)

Our objective is to define a deterministic mapping such that i.i.d. samples $x_0 \sim p_0$ passed through the mapping produce i.i.d. samples $x_1 \sim p_1$. We introduce Iterative α-(de)Blending (IADB), an iterative algorithm that can be implemented stochastically or deterministically. Our main result is that both variants converge toward the same limit, which yields a deterministic mapping between the densities p_0 and p_1, as shown in Figure 5.
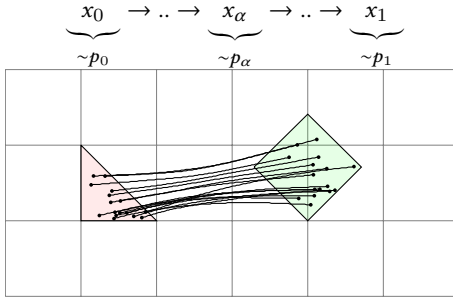

Fig. 5. **Iterative α-(de)blending**

*Algorithm 1: iterative α-(de)blending (*stochastic*).* Let's consider a number of iterations T and evenly distributed blending parameters $\alpha_t = t/T, t = \{0, .., T\})$. This algorithm creates a sequence $(x_{\alpha_t} \sim p_{\alpha_t}, t = \{0, .., T\})$ that starts with a random sample $x_0 \sim p_0$ and ends with a random sample $x_{\alpha_T} = x_1 \sim p_1$ by applying α-(de)blending iteratively. In each iteration, $x_{\alpha_t} \sim p_{\alpha_t}$ is α_t-deblended by sampling random posteriors, which are sampled and α_{t+1}-blended again to obtain a new sample $x_{\alpha_{t+1}} \sim p_{\alpha_{t+1}}$. End to end, this algorithm provides a stochastic mapping between samples $x_0 \sim p_0$ and samples $x_1 \sim p_1$.

Algorithm 1 Iterative α-(de)blending (stochastic)

Require: $x_0 \sim p_0$, T, $\alpha_t := \frac{t}{T}$
  for $t = 0, .., T - 1$ **do**
    sample $(x_0, x_1) \sim (p_0 \times p_1)_{|(x_{\alpha_t}, \alpha_t)}$
    $x_{\alpha_{t+1}} = (1 - \alpha_{t+1}) \, x_0 + \alpha_{t+1} \, x_1$
  end for

---

*Algorithm 2: iterative α-(de)blending (*deterministic*).* This algorithm is the same as Algorithm 1 except that, in each iteration, the random posterior samples are replaced by their expectations. The algorithm is thus not stochastic but deterministic.

Algorithm 2 Iterative α-(de)blending (deterministic)

Require: $x_0 \sim p_0$, T, $\alpha_t := \frac{t}{T}$
  for $t = 0, .., T - 1$ **do**
    $(\bar{x}_0, \bar{x}_1) = \mathbb{E}_{(p_0 \times p_1)_{|(x_{\alpha_t}, \alpha_t)}} \left[(x_0, x_1) \right]$
    $x_{\alpha_{t+1}} = (1 - \alpha_{t+1}) \, \bar{x}_0 + \alpha_{t+1} \, \bar{x}_1$
  end for

Theorem: *convergence of iterative α-(de)blending.* If p_0 and p_1 are Riemann-integrable densities of finite variance, the sequences computed by Algorithm 1 and Algorithm 2 converge toward the same limit as the number of steps T increases, i.e., for any $\alpha \in [0, 1]$:

$$\lim_{T \to \infty} x_\alpha \text{ computed by Algorithm 1}(x_0, T)$$
$$= \lim_{T \to \infty} x_\alpha \text{ computed by Algorithm 2}(x_0, T). \qquad (1)$$

Proof. We provide a detailed proof in Appendix A of our supplemental. But intuitively, with each iteration, Algorithm 1 makes a small step $\Delta x_\alpha = (x_1 - x_0) \, \Delta \alpha$ along the segment given by random posterior samples. As the number of iterations increases, many small random steps average out, and the infinitesimal steps are described by an ODE that involves the expected posteriors, as in Algorithm 2:

$$dx_\alpha = (\bar{x}_1 - \bar{x}_0) \, d\alpha. \qquad (2)$$

Hence, as T increases, the update rule of Algorithm 1 converges toward that of Algorithm 2. This is shown in Figure 6.

Fig. 6. Both algorithms step iteratively by moving the samples along segments defined by their posterior densities. The difference is that Algorithm 1 uses segments between random posterior samples, which creates stochastic paths, while Algorithm 2 uses the segment between the average of the posterior samples, which creates deterministic paths. As the number of steps T increases, the randomness of the stochastic paths averages out and they converge toward the deterministic paths.

Eric Heitz, Laurent Belcour, and Thomas Chambon

Connection to computer graphics applications. Figures 7 and 8 show how the mapping behaves in 2D. The deterministic mapping defined by the limit of the algorithm is a transport map (also called an area-preserving parameterization) that could potentially be of interest for common computer graphics applications such as parameterizing, sampling, and stippling. We believe that showing the connection is interesting, but our point here is not to make competitive claims for these applications. Instead, our focus is on using this mapping for deterministic denoising diffusion, as presented in Section 4.
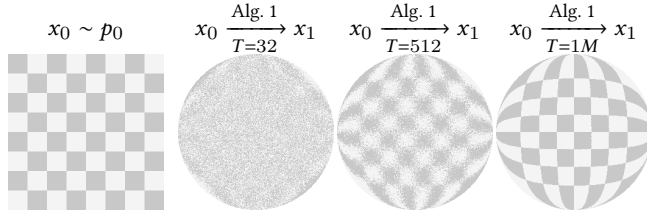

Fig. 7. **Stochastic mapping with Algorithm 1.** We map a uniform density on a square (p_0) and to a uniform density on a disk (p_1). The checkerboard pattern shows the randomness of the resulting mapping. The larger the number of steps T, the more the mapping converges and reveals a smooth parameterization of the disk.
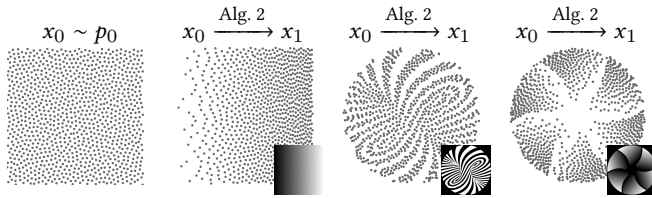

Fig. 8. **Deterministic mapping with Algorithm 2.** We use the deterministic mapping to warp blue-noise samples in the unit square to arbitrary densities.

4 LEARNING ITERATIVE α-(DE)BLENDING

In this section, we explain how to use iterative α-(de)blending in a machine learning context, where we train a neural network D_θ to predict the average posterior samples used in Algorithm 2.

4.1 Variant Formulations of Iterative α-(de)Blending

A direct transposition of Algorithm 2 means learning the averages of both posterior samples $\bar{x}_0$ and $\bar{x}_1$. However, one is implicitly given by the other such that it is not necessary to learn both, and variants of Alg. 2 are possible. The fact that multiple, theoretically equivalent, variants are possible is pointed out by Salimans and Ho [2022]. However, they are not equivalent in practice. In Table 1, we summarize four variants derived in Appendix B of our supplemental and compare their practical properties. Variant (a) is the vanilla transposition of Algorithm 2. It is highly unstable because instead of being a numerical update of the current sample x_{α_t}, the new sample $x_{\alpha_{t+1}}$ is computed from the outputs of the neural network. The residual learning errors of the network accumulate at each

step and the larger the number of steps T, the more this variant diverges. Variants (b) and (c) consist of learning either only $\bar{x}_0$ or $\bar{x}_1$. The sampling suffers from numerical instability near $\alpha_t = 0$ and $\alpha_t = 1$ because of the respective divisions by α_t and $1 - \alpha_t$. We recommend using variant (d), which consists of learning the average difference vector $\bar{x}_1 - \bar{x}_0$. It is a direct transposition of the ODE defined in Equation 2. This variant updates the current samples at each iteration without any division, making it the most stable variant for both training and sampling.

(a) **learn** $\bar{x}_0$ **and** $\bar{x}_1$	(b) **learn only** $\bar{x}_0$	(c) **learn only** $\bar{x}_1$	(d) **learn** $\bar{x}_1 - \bar{x}_0$
$(\bar{x}_0, \bar{x}_1) = D_\theta\left(x_{\alpha_t}, \alpha_t\right)$	$\bar{x}_0 = D_\theta\left(x_{\alpha_t}, \alpha_t\right)$	$\bar{x}_1 = D_\theta\left(x_{\alpha_t}, \alpha_t\right)$	$\bar{x}_1 - \bar{x}_0 = D_\theta\left(x_{\alpha_t}, \alpha_t\right)$
$x_{\alpha_{t+1}} =$	$x_{\alpha_{t+1}} = \bar{x}_0 +$	$x_{\alpha_{t+1}} = \bar{x}_1 +$	$x_{\alpha_{t+1}} = x_{\alpha_t} +$
$(1 - \alpha_{t+1})\,\bar{x}_0 + \alpha_{t+1}\bar{x}_1$	$\frac{\alpha_{t+1}}{\alpha_t}\left(x_{\alpha_t} - \bar{x}_0\right)$	$\frac{(1-\alpha_{t+1})}{(1-\alpha_t)}\left(x_{\alpha_t} - \bar{x}_1\right)$	$(\alpha_{t+1} - \alpha_t)\,(\bar{x}_1 - \bar{x}_0)$
unstable	unstable when $\alpha_t \to 0$	unstable when $\alpha_t \to 1$	stable

Table 1. **Variant formulations of iterative α-(de)blending** (equivalent in theory but not in practice).

4.2 Training and Sampling

Following variant (d) of Table 1, we train the neural network D_θ to predict the average difference vector between the posterior samples. Our learning objective is defined by

$$\min_\theta \ \mathbb{E}_{\alpha, x_\alpha}\left[\left\|D_\theta\left(x_\alpha, \alpha\right) - \mathbb{E}_{(x_0, x_1)_{|(x_\alpha, \alpha)}}\left[x_1 - x_0\right]\right\|^2\right]. \quad (3)$$

Note that minimizing the l^2 norm of the average of a distribution is equivalent to minimizing the l^2 norm of all of the samples of the distribution. We obtain the equivalent objective

$$\min_\theta \ \mathbb{E}_{\alpha, x_\alpha, (x_0, x_1)_{|(x_\alpha, \alpha)}}\left[\|D_\theta\left(x_\alpha, \alpha\right) - (x_1 - x_0)\|^2\right]. \quad (4)$$

Finally, as explained in Section 2, sampling $x_\alpha \sim p_\alpha$ first and then $(x_0, x_1)_{|(x_\alpha, \alpha)}$ is equivalent to sampling $(x_0, x_1) \sim (p_0, p_1)$ and blending them to obtain $x_\alpha \sim p_\alpha$. With this, we obtain our final learning objective

$$\min_\theta \ \mathbb{E}_{\alpha, x_0, x_1}\left[\|D_\theta\left((1 - \alpha)\,x_0 + \alpha\,x_1, \alpha\right) - (x_1 - x_0)\|^2\right], \quad (5)$$

which we use to optimize θ in Algorithm 3. In Algorithm 4, we iteratively map samples $x_0 \sim p_0$ to samples $x_1 \sim p_1$ in the same way as in Algorithm 2, where we use the neural network D_θ to obtain the average posterior difference.

Algorithm 3 Training

Require: $x_0 \sim p_0, x_1 \sim p_1, \alpha \sim \mathcal{U}_{[0,1]}$
$\quad x_\alpha = (1 - \alpha)\,x_0 + \alpha\,x_1$
$\quad l = \|D_\theta\left(x_\alpha, \alpha\right) - (x_1 - x_0)\|^2$
$\quad$ backprop from l and update θ

Algorithm 4 Sampling

Require: $x_0 \sim p_0, T, \alpha_t := \frac{t}{T}$
$\quad$ **for** $t = 0, .., T - 1$ **do**
$\quad\quad x_{\alpha_{t+1}} = x_{\alpha_t} + (\alpha_{t+1} - \alpha_t)\,D_\theta\left(x_{\alpha_t}, \alpha_t\right)$
$\quad$ **end for**

---

5 EXPERIMENTS WITH ANALYTIC DENSITIES

Experiments with 1D densities. In Figure 9, we experiment with analytic 1D densities, where the expectation $\bar{x}_1 - \bar{x}_0$ can be computed analytically rather than being learnt by a neural network D_θ. The experiment confirms that the analytic version matches the reference and that the neural network trained with the l_2 norm approximates the same mapping. We also tested training the neural network with the l_1 norm, which makes the neural network approximate the median of $x_1 - x_0$ rather than its average. The resulting mapping does not match the reference. This confirms that learning the average via l_2 training is a key component of our model, as explained in Section 4.2.

Experiments with 2D densities. Figure 10 shows that the intermediate blended densities p_α computed by our mapping match the reference blended densities. Figure 11 shows how our algorithm maps the samples of p_0 to samples of p_1. These results demonstrate that IADB computes valid mappings between arbitrary densities.

6 EXPERIMENTS WITH IMAGE DENSITIES

6.1 Gaussian sampling: comparison against DDIM

The state-of-the-art deterministic denoising diffusion model is DDIM [Song et al. 2021a]. The derivation of DDIM is based on the assumption that the first density is Gaussian. In this section, we show that if p_0 is Gaussian then IADB produces the same mapping as DDIM but with a different parameterization (a given x_0 is mapped to the same x_1 but the trajectory is different).

Proposition. If p_0 is a Gaussian density, IADB and DDIM define the same deterministic mapping.

Proof. In Appendix C of our supplemental, we show that, with a simple change of parameterization, the update rule of DDIM corresponds to variant (b) in Table 1.

IADB consistently outperforms DDIM in FID scores. In Figure 12, we experiment under the same conditions (architecture, training time, 1st-order solver, uniform schedule, Gaussian p_0) and measure the FID score [Heusel et al. 2017] for a varying number of sampling steps on 3 image datasets: LSUN Bedrooms (64x64), CelebA (64 x 64) and AFHQ Cats(128x128). We use a U-Net architecture from the HuggingFace Diffusers library[1]. The model has 6 downsampling blocks, 6 upsampling blocks, and a self-attention middle block. We trained the model with the AdamW optimizer (Learning rate=0.0001, Weight decay=0.01, betas=(0.9,0.999)) and we set the batch size to 64 for Celeba, 8 for AFHQ Cats, 64 for bedrooms, and 128 for Cifar. All models are trained for 120 hours of training (approx. 800k steps on the CelebA dataset) on a single NVIDIA Titan RTX. We observe a consistently better performance with IADB compared to DDIM.

Discussion. The improved performance of IADB compared to DDIM is due to multiple factors. The formulation generally used in DDIM corresponds to variant (b) presented in Table 1: they train a denoiser to predict the Gaussian noise present in the noisy image samples, i.e., their model learns to predict $\bar{x}_0$. However, we explain that this variant makes the sampling less stable because of the

---

[1]https://github.com/huggingface/diffusers

division near 0. As a matter of fact, in their implementation, the sampler starts at some $\epsilon > 0$ precisely to avoid dividing by 0. Our variant (d) does not suffer from this problem. Another factor is that the learning objective defined by variant (d) provides a better optimization landscape than variant (b). For instance, the effort to learn $\bar{x}_0$ in variant (b) is imbalanced over α because the l^2 norm is small near $\alpha = 0$ and large near $\alpha = 1$. In contrast, the effort to learn $\bar{x}_1 - \bar{x}_0$ in variant (d) is more balanced over α.

6.2 Non-Gaussian sampling

In contrast to DDIM, IADB does not make the assumption that p_0 is Gaussian. Indeed, IADB is theoretically proven to produce a correct sampling of p_1 for *any* p_0 (as long as they are Riemann integrable and of finite variance). In this section, we experiment with how IADB behaves with non-Gaussian densities for p_0.

Impact on sampling quality. In the experiment of Figure 13, we use IADB to sample face images (p_1) using different densities for p_0. We observe that IADB does indeed generate faces regardless of the choice of p_0. However, while we observe a similar sampling quality for analytic p_0 (Gaussian, uniform and bi-Gaussian noises), we see a significant drop in quality when p_0 is not an analytic primitive but a real-image dataset such as the pebble textures. This observation does not invalidate the theory: IADB effectively defines a valid mapping between the pebble density p_0 and the face density p_1, but the quality achieved is lower in practice. We conjecture that this is because the learning task is more difficult. Indeed, the analytic noise primitives provide a simple and smooth landscape for p_0 such that the learning capacity of the neural network can be entirely spent on learning the p_1 manifold. In contrast, when p_0 is also a complex image manifold, the learning capacity of the network is spent on both p_0 and p_1. This might explain the lower quality when generating samples from p_1.

Correct but unfaithful mappings. Figure 14 shows an experiment where we use IADB to sample color face images (p_1) using grayscale face images (p_0). We observe that IADB successfully accomplishes this task: it effectively maps grayscale faces to color faces. Unfortunately, the output color images are not colorizations of the input grayscale images, which rules out some user applications. However, this is not the promise of the theory. Indeed, the theory predicts that the mapping produces a valid sampling of p_1 using p_0 (which is the case in the experiment) but not that the mapping will be what a user expects (which is not the case in the experiment).

Faithful mappings with conditional IADB. Previous works show that conditioning the diffusion process seems to be necessary for achieving faithful image-to-image translations. For instance, adding an energy guide during the ODE integration [Zhao et al. 2022] by progressively injecting features [Meng et al. 2021] or by sampling conditional densities Saharia et al. [2022a, 2021]. In Figure 15, we experiment with the latter using Gaussian noise for x_0, clean images for x_1, and a corrupted version of x_1 for the condition c passed as an additional argument to the neural network: $D_\theta(c, x_\alpha, \alpha) = \bar{x}_1 - \bar{x}_0$. The experiment shows that IADB can be successfully used to obtain faithful image-to-image translations with additional conditioning.

7 DISCUSSION

Improved sampler. We experimented with IADB in its vanilla setting with a uniform blending schedule and a first-order ODE solver. It readily benefits from orthogonal improvements brought to denoising diffusion, such as better blending schedules and higher-order ODE solvers [Karras et al. 2022]. For instance, Algorithm 5 provides an improved version of Algorithm 4 with a 2nd-order Runge-Kutta integration and a cosine schedule.

Algorithm 5 Sampling (2nd-order Runge-Kutta, cosine schedule)

Require: $x_0 \sim p_0$, T, $\alpha_t := 1 - \cos\left(\frac{t}{T} \frac{\pi}{2}\right)$

    for $t = 0, .., T - 1$ **do**

        $x_{\alpha_{t+\frac{1}{2}}} = x_{\alpha_t} + \left(\alpha_{t+\frac{1}{2}} - \alpha_t\right) D_\theta\left(x_{\alpha_t}, \alpha_t\right)$

        $x_{\alpha_{t+1}} = x_{\alpha_t} + \left(\alpha_{t+1} - \alpha_t\right) D_\theta\left(x_{\alpha_{t+\frac{1}{2}}}, \alpha_{t+\frac{1}{2}}\right)$

    end for

Stochastic Differential Equations (SDEs). The random sequence computed by the stochastic version of IADB presented in Algorithm 1 is a Markov chain. This algorithm might therefore appear reminiscent of stochastic diffusion models [Song et al. 2021b] based on SDEs. However, IADB is not related to an SDE. Indeed, SDEs model stochastic behaviors at the infinitesimal scale while our mapping is stochastic for discrete steps and becomes a deterministic ODE in the infinitesimal limit.

Non-Gaussian denoising diffusion. Some previous works have focused on replacing Gaussian noise with other noise distributions, such as the generalised normal (exponential power) distribution [Deasy et al. 2021] or the Gamma distribution [Nachmani et al. 2021]. Our more general derivation works with any finite-variance density rather than specific noise alternatives. Peluchetti [2022] proposes a more general SDE framework. Our ODE can be derived from his SDE by nullifying the stochastic component and following its aggregation method. In this respect, our ODE is not entirely new. However, our derivation is new and incomparably simpler, which is the main point of this paper.

8 CONCLUSION

The objective of this work was to find a simple and intuitive way to approach deterministic denoising diffusion. Using only simple sampling concepts, we derived Iterative α-(De)Blending (IADB), a deterministic diffusion model based on a sampling interpretation of blending and deblending. We have seen that our model defines exactly the same mapping as DDIM [Song et al. 2021a], the state-of-the-art competitor in deterministic denoising diffusion. This yields a positive answer to the question asked in the introduction *"Is there a simpler approach to deterministic diffusion?"*. Indeed, it is possible to derive the same result without leveraging any knowledge about Langevin dynamics, score matching, SDEs, etc. Getting there was the whole point of this paper. Furthermore, our simpler IADB derivation provides both practical and theoretical gains. It has led to a more numerically stable formulation that produces better FID scores than DDIM and has revealed that DDIM's Gaussian assumption is theoretically unnecessary.

REFERENCES

Jacob Deasy, Nikola Simidjievski, and Pietro Liò. 2021. Heavy-tailed denoising score matching. *ArXiv* abs/2112.09788 (2021).

Prafulla Dhariwal and Alexander Quinn Nichol. 2021. Diffusion Models Beat GANs on Image Synthesis. *Advances in Neural Information Processing Systems* 34.

Martin Heusel, Hubert Ramsauer, Thomas Unterthiner, Bernhard Nessler, and Sepp Hochreiter. 2017. Gans trained by a two time-scale update rule converge to a local nash equilibrium. *Advances in neural information processing systems* 30 (2017).

Jonathan Ho, Ajay Jain, and Pieter Abbeel. 2020. Denoising Diffusion Probabilistic Models. *Advances in Neural Information Processing Systems* 32 (2020).

Jonathan Ho, Tim Salimans, Alexey Gritsenko, William Chan, Mohammad Norouzi, and David J. Fleet. 2022. Video Diffusion Models. arXiv:2204.03458 [cs.CV]

Tero Karras, Miika Aittala, Timo Aila, and Samuli Laine. 2022. Elucidating the Design Space of Diffusion-Based Generative Models.

Tero Karras, Miika Aittala, Samuli Laine, Erik Härkönen, Janne Hellsten, Jaakko Lehtinen, and Timo Aila. 2021. Alias-Free Generative Adversarial Networks. In *Proc. NeurIPS*.

Tero Karras, Samuli Laine, Miika Aittala, Janne Hellsten, Jaakko Lehtinen, and Timo Aila. 2020. Analyzing and Improving the Image Quality of StyleGAN. In *2020 IEEE/CVF Conference on Computer Vision and Pattern Recognition (CVPR)*. 8107–8116.

Bahjat Kawar, Michael Elad, Stefano Ermon, and Jiaming Song. 2022. Denoising Diffusion Restoration Models. *arXiv preprint arXiv:2201.11793* (2022).

Zhifeng Kong, Wei Ping, Jiaji Huang, Kexin Zhao, and Bryan Catanzaro. 2020. DiffWave: A Versatile Diffusion Model for Audio Synthesis.

Chenlin Meng, Yang Song, Jiaming Song, Jiajun Wu, Jun-Yan Zhu, and Stefano Ermon. 2021. Sdedit: Image synthesis and editing with stochastic differential equations. *arXiv preprint arXiv:2108.01073* (2021).

Eliya Nachmani, Robin San Roman, and Lior Wolf. 2021. Denoising Diffusion Gamma Models. arXiv:2110.05948 [eess.SP]

Alexander Quinn Nichol and Prafulla Dhariwal. 2021. Improved Denoising Diffusion Probabilistic Models. In *Proceedings of the 38th International Conference on Machine Learning (Proceedings of Machine Learning Research, Vol. 139)*. 8162–8171.

Stefano Peluchetti. 2022. Non-Denoising Forward-Time Diffusions. https://openreview.net/forum?id=oVfIKuhqfC

Thomas Porter and Tom Duff. 1984. Compositing Digital Images. *SIGGRAPH Comput. Graph.* 18, 3 (1984), 253–259.

Aditya Ramesh, Prafulla Dhariwal, Alex Nichol, Casey Chu, and Mark Chen. 2022. Hierarchical Text-Conditional Image Generation with CLIP Latents. arXiv:2204.06125 [cs.CV]

Robin Rombach, Andreas Blattmann, Dominik Lorenz, Patrick Esser, and Björn Ommer. 2021. High-Resolution Image Synthesis with Latent Diffusion Models.

Chitwan Saharia, William Chan, Huiwen Chang, Chris Lee, Jonathan Ho, Tim Salimans, David Fleet, and Mohammad Norouzi. 2022a. Palette: Image-to-Image Diffusion Models. In *ACM SIGGRAPH 2022 Conference Proceedings*. Article 15, 10 pages.

Chitwan Saharia, William Chan, Saurabh Saxena, Lala Li, Jay Whang, Emily Denton, Seyed Kamyar Seyed Ghasemipour, Burcu Karagol Ayan, S. Sara Mahdavi, Rapha Gontijo Lopes, Tim Salimans, Jonathan Ho, David J Fleet, and Mohammad Norouzi. 2022b. Photorealistic Text-to-Image Diffusion Models with Deep Language Understanding.

Chitwan Saharia, Jonathan Ho, William Chan, Tim Salimans, David J. Fleet, and Mohammad Norouzi. 2021. Image Super-Resolution via Iterative Refinement. *arXiv preprint arXiv:2104.07636* (2021).

Tim Salimans and Jonathan Ho. 2022. Progressive Distillation for Fast Sampling of Diffusion Models. In *International Conference on Learning Representations*. https://openreview.net/forum?id=TIdIXIpzhoI

Jiaming Song, Chenlin Meng, and Stefano Ermon. 2021a. Denoising Diffusion Implicit Models. *International Conference on Learning Representations* (2021).

Yang Song and Stefano Ermon. 2019. Generative modeling by estimating gradients of the data distribution. *Advances in Neural Information Processing Systems* 32 (2019).

Yang Song and Stefano Ermon. 2020. Improved Techniques for Training Score-Based Generative Models. *ArXiv* abs/2006.09011 (2020).

Yang Song, Jascha Sohl-Dickstein, Diederik P. Kingma, Abhishek Kumar, Stefano Ermon, and Ben Poole. 2021b. Score-Based Generative Modeling through Stochastic Differential Equations. *International Conference on Learning Representations* (2021).

Pascal Vincent. 2011. A Connection Between Score Matching and Denoising Autoencoders. *Neural Computation* 23, 7 (2011), 1661–1674.

Jay Whang, Mauricio Delbracio, Hossein Talebi, Chitwan Saharia, Alexandros G Dimakis, and Peyman Milanfar. 2022. Deblurring via stochastic refinement. In *Proceedings of the IEEE/CVF Conference on Computer Vision and Pattern Recognition*. 16293–16303.

Min Zhao, Fan Bao, Chongxuan Li, and Jun Zhu. 2022. Egsde: Unpaired image-to-image translation via energy-guided stochastic differential equations. *arXiv preprint arXiv:2207.06635* (2022).
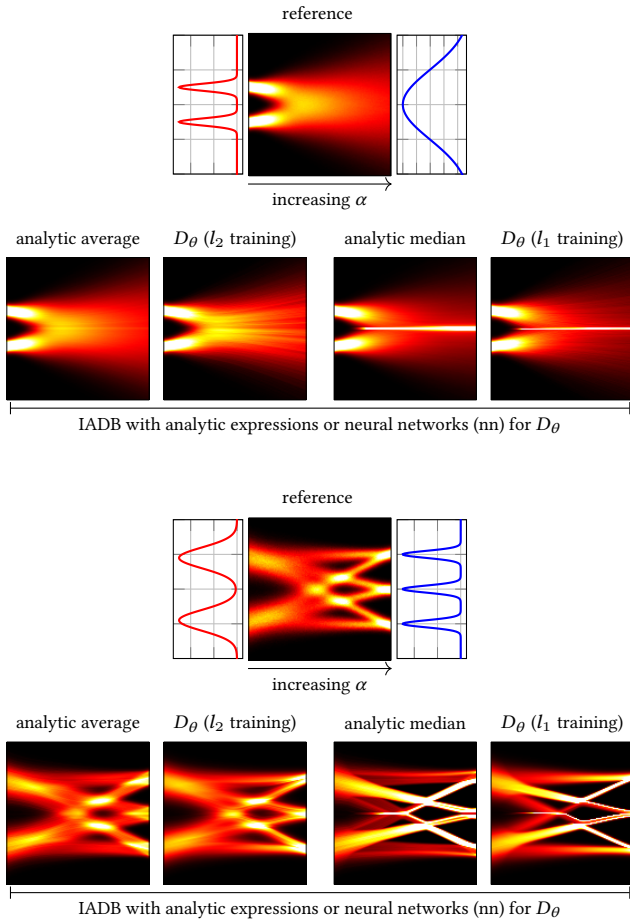
reference

increasing α

analytic average $\quad D_\theta$ (l_2 training) $\quad$ analytic median $\quad D_\theta$ (l_1 training)

IADB with analytic expressions or neural networks (nn) for D_θ

reference

increasing α

analytic average $\quad D_\theta$ (l_2 training) $\quad$ analytic median $\quad D_\theta$ (l_1 training)

IADB with analytic expressions or neural networks (nn) for D_θ

Fig. 9. **Experiments with 1D densities.** (top) We blend a bi-Normal distribution with modes $\mu_{1|2} = \{-0.5, 0.5\}$ and $\sigma_{1|2} = 0.1$ (in red) with a Normal distribution of unit variance (in blue). (bottom) We blend a bi-Normal distribution with modes $\mu_{1|2} = \{-0.9, 0.9\}$ and $\sigma_{1|2} = 0.3$ (in red) to a tri-Normal distribution with $\mu_{1|2|3} = \{-1, 0, 1\}$ and $\sigma_{1|2|3} = 0.1$ (in blue). The reference shows analytically convolved densities p_α. The other densities are the histograms of the samples x_α computed in Algorithm 4 using either analytic expressions or neural networks for D_θ. The neural network is an MLP with 5 hidden layers of 64 filters trained with the Adam optimizer with a learning rate of 10^{-5} for 10k iterations.
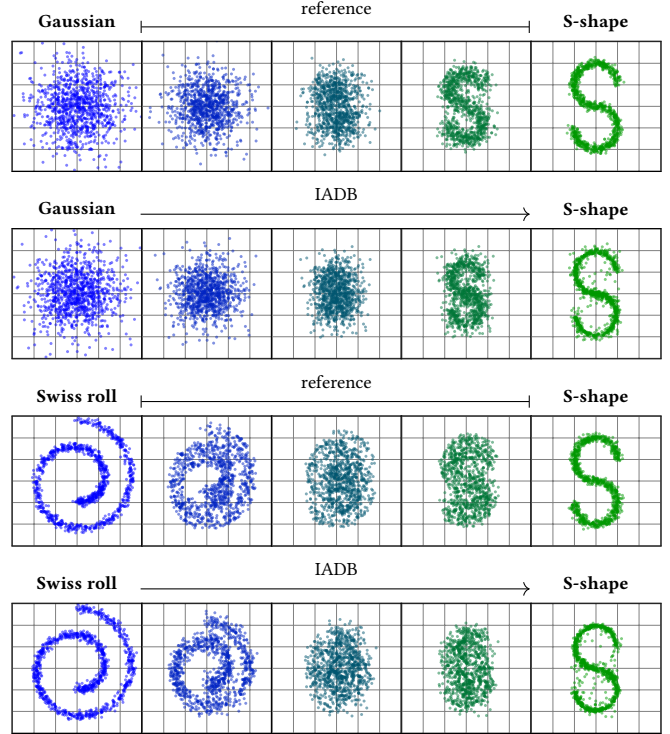
Fig. 10. **Experiments with 2D densities: intermediate distributions.** We show samples of the intermediate densities p_α. References are computed by α-blending random samples from p_0 and p_1. IADB intermediate distributions are computed with Algorithm 4 using an MLP with 5 hidden layers of 64 filters for D_θ trained with the Adam optimizer with a learning rate of 10^{-5} for 10k iterations.
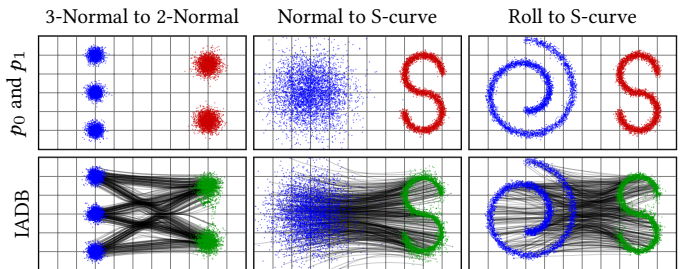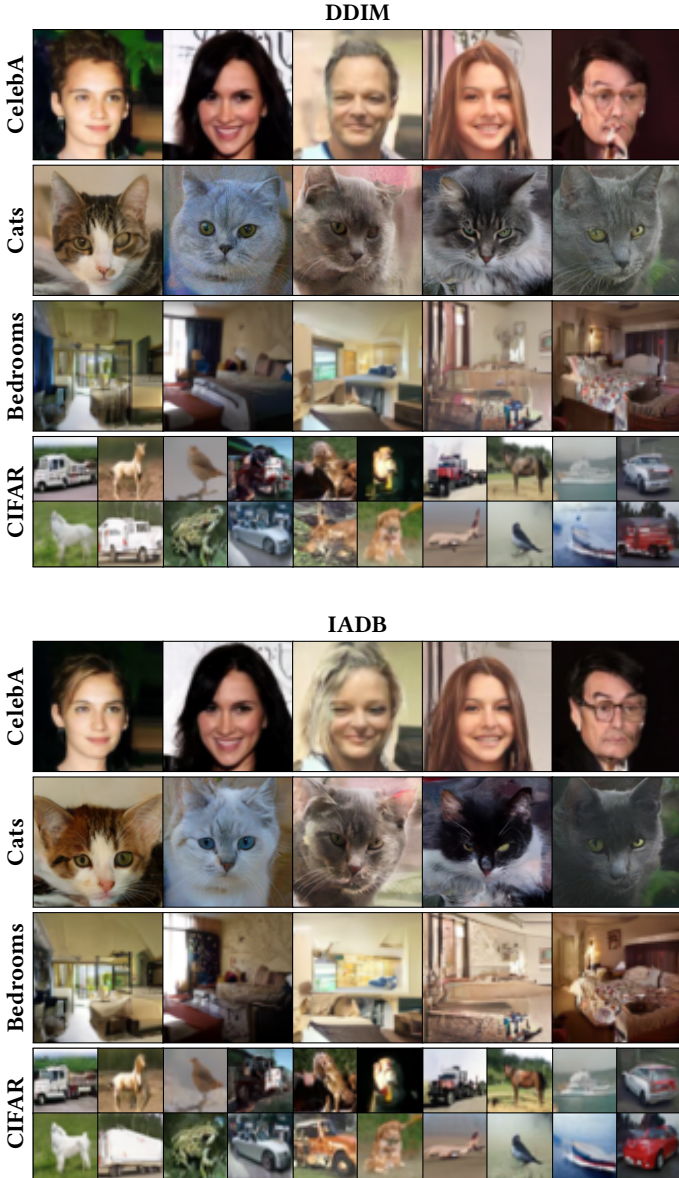
Fig. 11. **Experiments with 2D densities: mappings.** We show samples of the reference densities p_0 and p_1 and the mapping computed by Algorithm 4 using an MLP with 5 hidden layers of 64 filters for D_θ trained with the Adam optimizer with a learning rate of 10^{-5} for 10k iterations. The final samples computed by the algorithm (green) match the reference samples x_1 (red).

DDIM

IADB

	$T=2$	$T=4$	$T=8$	$T=16$	$T=32$	$T=128$
Cats DDIM	200.89	39.32	22.98	18.12	13.66	9.26
IADB	**86.68**	39.40	**17.50**	**11.15**	**8.06**	**6.69**
CelebA DDIM	177.86	46.58	**19.50**	**11.91**	9.23	6.93
IADB	**108.13**	51.79	22.68	12.15	**7.52**	**5.56**
Bedrooms DDIM	307.76	104.55	38.58	24.26	20.34	16.82
IADB	**238.45**	**57.60**	**18.55**	**14.12**	**14.57**	15.93
CIFAR DDIM	174.54	58.53	20.92	11.01	7.74	6.20
IADB	**157.32**	**50.69**	**16.74**	**8.73**	**6.45**	**5.61**

Fig. 12. **Comparing IADB and DDIM.** We use the same Gaussian noise to sample images with IADB and DDIM. We obtain very close images because the underlying theoretical mappings are the same. IADB achieves better FID scores w.r.t. the number of steps T than DDIM most of the time.
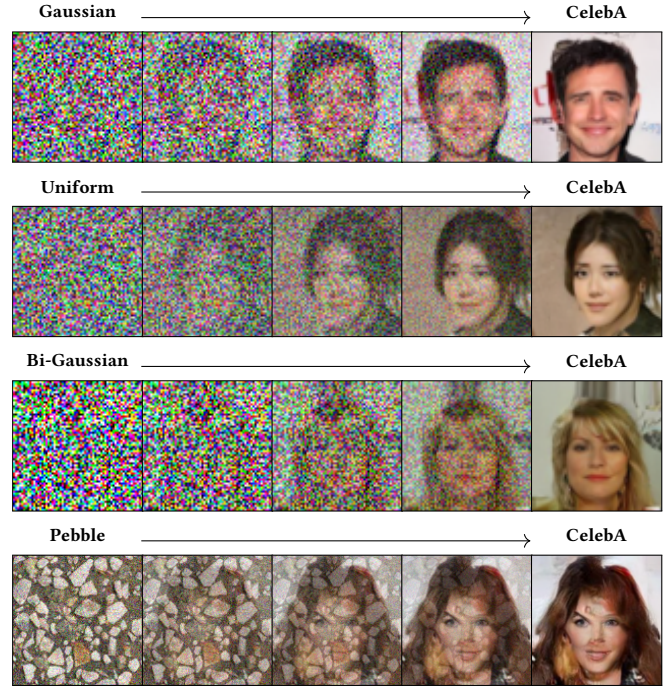

Fig. 13. **Mapping arbitrary image densities.** We use the same experimental set up as in Figure 12 except that we also try uniform noise, bi-Gaussian noise and a pebble-texture dataset for p_0.
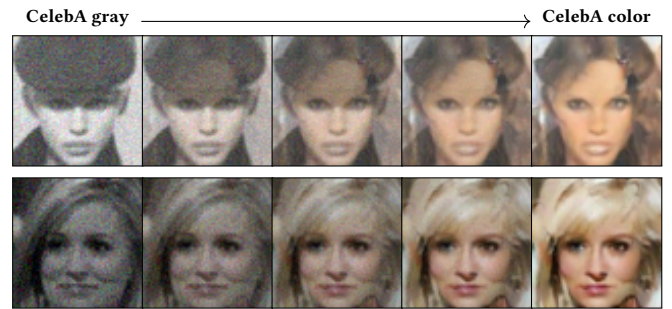

Fig. 14. **Image restoration with IADB.** In this experiment, we use IADB to map grayscale images to color images. The mapping creates a clean image but it does not match the grayscale one.
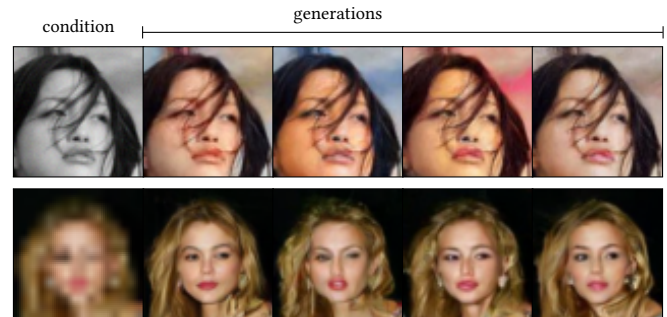

Fig. 15. **Conditional image restoration with IADB.** From a corrupt image (the condition), either decolorization (top) or downscaling (down), we create various restorations using different Gaussian noises x_0.

A CONVERGENCE OF ITERATIVE α-(DE)BLENDING

A.1 Preliminaries

We first recall some properties that are required in the derivation of the limit of Algorithm 1.

The posterior distributions have finite variance. The theorem requires that p_0 and p_1 are of finite variance, such that their respective posterior densities $p_{0|(x,\alpha)}$ and $p_{1|(x,\alpha)}$ are also of finite variance. This is because the idea of the proof is that averaging many small random steps (provided by the posterior distributions) converges toward their expectations and it is true only if their variance is finite. We use this between Equation (21) and Equation (22).

The expectations of the posterior distributions are continuous. If p_0 and p_1 are classic Riemann-integrable densities, then they are continuous almost everywhere. Since the blended distributions are essentially convolutions of p_0 and p_1, it follows that the posterior densities $p_{0|(x,\alpha)}$ and $p_{1|(x,\alpha)}$ are also continuous almost everywhere, and the expectation of their samples $x_{0|(x,\alpha)} \sim p_{0|(x,\alpha)}$ and $x_{1|(x,\alpha)} \sim p_{1|(x,\alpha)}$ are continuous everywhere (the expectation cancels out the null set where they are not continuous). In summary, for any $x \in \mathbb{R}^d$ and $\alpha \in [0,1]$ we have:

$$\lim_{x' \to x} \mathbb{E}\left[x_{0|(x',\alpha)}\right] = \mathbb{E}\left[x_{0|(x,\alpha)}\right], \lim_{x' \to x} \mathbb{E}\left[x_{1|(x',\alpha)}\right] = \mathbb{E}\left[x_{1|(x,\alpha)}\right], \tag{6}$$

$$\lim_{\alpha' \to \alpha} \mathbb{E}\left[x_{0|(x,\alpha')}\right] = \mathbb{E}\left[x_{0|(x,\alpha)}\right], \lim_{\alpha' \to \alpha} \mathbb{E}\left[x_{1|(x,\alpha)}\right] = \mathbb{E}\left[x_{1|(x,\alpha)}\right]. \tag{7}$$

We use this between Equation (22) and Equation (23).

A.2 Objective of the proof

To prove that Algorithm 1 and Algorithm 2 converge toward the same limit as the number of steps T increases, we need to show that the trajectories of the samples are the same. This is the case if, in the limit, the derivatives $\frac{dx_\alpha}{d\alpha}$ are the same with both algorithms. The discrete update at step t is:

$$\Delta\alpha_t = \alpha_{t+1} - \alpha_t = \frac{1}{T}, \tag{8}$$

$$\Delta x_{\alpha_t} = x_{\alpha_{t+1}} - x_{\alpha_t}, \tag{9}$$

and we want to prove that for any $\alpha \in [0,1]$ and at point $x_\alpha \in \mathbb{R}^d$ the continuous limit exists and is the same with both algorithms:

$$\frac{dx_\alpha}{d\alpha} = \lim_{\Delta\alpha \to 0} \frac{\Delta x_\alpha}{\Delta\alpha}. \tag{10}$$

A.3 Limit of Algorithm 2.

In step t of Algorithm 2, we use the average of the posterior samples that are such that

$$x_{\alpha_t} = (1-\alpha_t)\bar{x}_{0|(x_{\alpha_t},\alpha_t)} + \alpha_t \bar{x}_{1|(x_{\alpha_t},\alpha_t)}, \tag{11}$$

$$x_{\alpha_{t+1}} = (1-\alpha_{t+1})\bar{x}_{0|(x_{\alpha_t},\alpha_t)} + \alpha_{t+1}\bar{x}_{1|(x_{\alpha_t},\alpha_t)}, \tag{12}$$

where Equation (11) is a property of the average posteriors of x_{α_t} and Equation (12) is true by definition in Algorithm 2. We thus have the discrete difference

$$\Delta x_{\alpha_t} = x_{\alpha_{t+1}} - x_{\alpha_t} = \Delta\alpha_t\left(\bar{x}_{1|(x_{\alpha_t},\alpha_t)} - \bar{x}_{0|(x_{\alpha_t},\alpha_t)}\right). \tag{13}$$

We obtain the discrete ratio

$$\frac{\Delta x_\alpha}{\Delta\alpha} = \bar{x}_{1|(x_\alpha,\alpha)} - \bar{x}_{0|(x_\alpha,\alpha)}, \tag{14}$$

which is independent of $\Delta\alpha$. The limit hence exists and is defined by

$$\boxed{\frac{dx_\alpha}{d\alpha} = \lim_{\Delta\alpha \to 0}\frac{\Delta x_\alpha}{\Delta\alpha} = \frac{\Delta x_\alpha}{\Delta\alpha} = \bar{x}_{1|(x_\alpha,\alpha)} - \bar{x}_{0|(x_\alpha,\alpha)}.} \tag{15}$$

A.4 Limit of Algorithm 1.

In step t of Algorithm 1, we sample random posterior samples $x_{0|(x_{\alpha_t},\alpha_t)}$ and $x_{1|(x_{\alpha_t},\alpha_t)}$ that are such that

$$x_{\alpha_t} = (1-\alpha_t)x_{0|(x_{\alpha_t},\alpha_t)} + \alpha_t x_{1|(x_{\alpha_t},\alpha_t)}, \tag{16}$$

$$x_{\alpha_{t+1}} = (1-\alpha_{t+1})x_{0|(x_{\alpha_t},\alpha_t)} + \alpha_{t+1}x_{1|(x_{\alpha_t},\alpha_t)}, \tag{17}$$

where Equation (16) is a property of the posteriors of x_{α_t} and Equation (17) is true by definition in Algorithm 1. We thus have the discrete difference

$$\Delta x_{\alpha_t} = x_{\alpha_{t+1}} - x_{\alpha_t} = \Delta\alpha_t\left(x_{1|(x_{\alpha_t},\alpha_t)} - x_{0|(x_{\alpha_t},\alpha_t)}\right). \tag{18}$$

We obtain the discrete difference for any parameter $\alpha \in [0,1]$ and any location $x_\alpha \in \mathbb{R}^d$

$$\Delta x_\alpha = \Delta\alpha\left(x_{1|(x_\alpha,\alpha)} - x_{0|(x_\alpha,\alpha)}\right). \tag{19}$$

Furthermore, increasing the number of steps is equivalent to decomposing each step $\Delta\alpha$ into N smaller steps $\Delta\alpha/N$. We rewrite the discrete difference as

$$\Delta x_\alpha = \frac{\Delta\alpha}{N}\sum_{n=0}^{N-1}\left(x_{1|(x_{\alpha+n\Delta\alpha/N},\alpha+n\Delta\alpha/N)} - x_{0|(x_{\alpha+n\Delta\alpha/N},\alpha+n\Delta\alpha/N)}\right). \tag{20}$$

With this modification, if the derivative exists, it is defined by the limit

$$\frac{dx_\alpha}{d\alpha} = \lim_{\Delta\alpha \to 0}\lim_{N \to \infty}\frac{\Delta x_\alpha}{\Delta\alpha} = \lim_{\Delta\alpha \to 0}\lim_{N \to \infty}$$
$$\frac{1}{N}\sum_{n=0}^{N-1}\left(x_{1|(x_{\alpha+n\Delta\alpha/N},\alpha+n\Delta\alpha/N)} - x_{0|(x_{\alpha+n\Delta\alpha/N},\alpha+n\Delta\alpha/N)}\right). \tag{21}$$

Thanks to the **finite-variance** condition of p_0 and p_1, the normalized average sum converges toward the average of the posterior samples over $\alpha' \in [\alpha, \alpha+\Delta\alpha]$ as N increases.

$$\frac{dx_\alpha}{d\alpha} = \lim_{\Delta\alpha \to 0}\mathop{\mathbb{E}}_{\alpha' \in [\alpha,\alpha+\Delta\alpha]}\left[x_{1|(x_{\alpha'},\alpha')}\right] - \mathop{\mathbb{E}}_{\alpha' \in [\alpha,\alpha+\Delta\alpha]}\left[x_{0|(x_{\alpha'},\alpha')}\right]. \tag{22}$$

Finally, because **the expectations of the posterior densities are continuous**, we obtain that the expectations over $[\alpha, \alpha+\Delta\alpha]$ converge toward the expectation in α, such that

$$\boxed{\frac{dx_\alpha}{d\alpha} = \mathbb{E}\left[x_{1|(x_\alpha,\alpha)}\right] - \mathbb{E}\left[x_{0|(x_\alpha,\alpha)}\right] = \bar{x}_{1|(x_\alpha,\alpha)} - \bar{x}_{0|(x_\alpha,\alpha)}.} \tag{23}$$

This is the same result as in Equation (15) with Algorithm 2.

B VARIANT FORMULATIONS

We derive the variant formulations introduced in Section 4.

Blended samples. A blended sample is by definition the blending of its posterior samples

$$x_{\alpha_t} = (1 - \alpha_t) x_0 + \alpha_t x_1. \tag{24}$$

Since blending is linear, a blended sample is also the blending of the average of its posterior samples:

$$x_{\alpha_t} = (1 - \alpha_t) \bar{x}_0 + \alpha_t \bar{x}_1. \tag{25}$$

We can thus rewrite its average posteriors samples $\bar{x}_0$ and $\bar{x}_1$ in the following way:

$$\bar{x}_0 = \frac{x_{\alpha_t}}{1 - \alpha_t} - \frac{\alpha_t \bar{x}_1}{1 - \alpha_t}, \tag{26}$$

$$\bar{x}_1 = \frac{x_{\alpha_t}}{\alpha_t} - \frac{(1 - \alpha_t) \bar{x}_0}{\alpha_t}. \tag{27}$$

Variant (a): In the vanilla version of the algorithm, a blended sample of parameter α_{t+1} is obtained by blending $\bar{x}_0$ and $\bar{x}_1$:

$$x_{\alpha_{t+1}} = (1 - \alpha_{t+1}) \bar{x}_0 + \alpha_{t+1} \bar{x}_1. \tag{28}$$

Variant (b): By expanding $\bar{x}_1$ from Equation (28) using Equation (27), we obtain

$$
\begin{aligned}
x_{\alpha_{t+1}} &= (1 - \alpha_{t+1}) \bar{x}_0 + \alpha_{t+1} \bar{x}_1, \\
&= (1 - \alpha_{t+1}) \bar{x}_0 + \alpha_{t+1} \left(\frac{x_{\alpha_t}}{\alpha_t} - \frac{(1 - \alpha_t) \bar{x}_0}{\alpha_t} \right), \\
&= \left(1 - \alpha_{t+1} - \frac{\alpha_{t+1} (1 - \alpha_t)}{\alpha_t} \right) \bar{x}_0 + \frac{\alpha_{t+1}}{\alpha_t} x_{\alpha_t}, \\
&= \left(1 - \frac{\alpha_{t+1}}{\alpha_t} \right) \bar{x}_0 + \frac{\alpha_{t+1}}{\alpha_t} x_{\alpha_t}, \\
&= \bar{x}_0 + \frac{\alpha_{t+1}}{\alpha_t} \left(x_{\alpha_t} - \bar{x}_0 \right).
\end{aligned} \tag{29}
$$

Variant (c): By expanding $\bar{x}_0$ from Equation (28) using Equation (26), we obtain

$$
\begin{aligned}
x_{\alpha_{t+1}} &= (1 - \alpha_{t+1}) \bar{x}_0 + \alpha_{t+1} \bar{x}_1, \\
&= (1 - \alpha_{t+1}) \left(\frac{x_{\alpha_t}}{1 - \alpha_t} - \frac{\alpha_t \bar{x}_1}{1 - \alpha_t} \right) + \alpha_{t+1} \bar{x}_1, \\
&= \left(\alpha_{t+1} - \frac{(1 - \alpha_{t+1}) \alpha_t}{1 - \alpha_t} \right) \bar{x}_1 + \frac{1 - \alpha_{t+1}}{1 - \alpha_t} x_{\alpha_t}, \\
&= \left(1 - \frac{1 - \alpha_{t+1}}{1 - \alpha_t} \right) \bar{x}_1 + \frac{1 - \alpha_{t+1}}{1 - \alpha_t} x_{\alpha_t}, \\
&= \bar{x}_1 + \frac{1 - \alpha_{t+1}}{1 - \alpha_t} \left(x_{\alpha_t} - \bar{x}_1 \right).
\end{aligned} \tag{30}
$$

Variant (d): By rewriting $\alpha_{t+1} = \alpha_{t+1} + \alpha_t - \alpha_t$ in the definition of $x_{\alpha_{t+1}}$, we obtain

$$
\begin{aligned}
x_{\alpha_{t+1}} &= (1 - \alpha_{t+1}) \bar{x}_0 + \alpha_{t+1} \bar{x}_1, \\
&= (1 - \alpha_{t+1} + \alpha_t - \alpha_t) \bar{x}_0 + (\alpha_{t+1} + \alpha_t - \alpha_t) \bar{x}_1, \\
&= (1 - \alpha_t) \bar{x}_0 + \alpha_t \bar{x}_1 + (\alpha_{t+1} - \alpha_t) (\bar{x}_1 - \bar{x}_0), \\
&= x_{\alpha_t} + (\alpha_{t+1} - \alpha_t) (\bar{x}_1 - \bar{x}_0).
\end{aligned} \tag{31}
$$

C RELATION TO DDIM

In this section, we follow the notation of [Song et al. 2021a]: x_0 is a sample of a target density and ϵ is a random Gaussian sample. The denoiser of DDIM is defined such that, for an input $x_t = \sqrt{\alpha_t} x_0 + \sqrt{1 - \alpha_t}\epsilon$, it learns $\epsilon^{(t)}(x_t) = \bar{\epsilon}$. We define

$$y_t = \frac{x_t}{\sqrt{\alpha_t} + \sqrt{1 - \alpha_t}} = \beta_t x_0 + (1 - \beta_t) \epsilon, \tag{32}$$

where $\beta_t = \frac{\sqrt{\alpha_t}}{\sqrt{\alpha_t} + \sqrt{1 - \alpha_t}}$. y_t is an alpha-blended sample such as the one we defined in Section 3. It follows that we have

$$\frac{x_t}{\sqrt{\alpha_t}} = \frac{y_t}{\beta_t}. \tag{33}$$

We now turn to Equation (13) of [Song et al. 2021a]:

$$\frac{x_{t+1}}{\sqrt{\alpha_{t+1}}} = \frac{x_t}{\sqrt{\alpha_t}} + \left(\sqrt{\frac{1 - \alpha_{t+1}}{\alpha_{t+1}}} - \sqrt{\frac{1 - \alpha_t}{\alpha_t}} \right) \epsilon^{(t)}(x_t), \tag{34}$$

By injecting the scaled coordinate from Equation (33) into this expression, we obtain:

$$
\begin{aligned}
\frac{y_{t+1}}{\beta_{t+1}} &= \frac{y_t}{\beta_t} + \left(\sqrt{\frac{1 - \alpha_{t+1}}{\alpha_{t+1}}} - \sqrt{\frac{1 - \alpha_t}{\alpha_t}} \right) \bar{\epsilon} \\
\Rightarrow y_{t+1} &= y_t \frac{\beta_{t+1}}{\beta_t} + \frac{1}{\beta_t} \beta_t \beta_{t+1} \left(\sqrt{\frac{1 - \alpha_{t+1}}{\alpha_{t+1}}} - \sqrt{\frac{1 - \alpha_t}{\alpha_t}} \right) \bar{\epsilon}.
\end{aligned} \tag{35}
$$

Since

$$
\begin{aligned}
\beta_{t+1} \beta_t \left(\sqrt{\frac{1 - \alpha_{t+1}}{\alpha_{t+1}}} - \sqrt{\frac{1 - \alpha_t}{\alpha_t}} \right) &= \beta_t (1 - \beta_{t+1}) - (1 - \beta_t) \beta_{t+1}, \\
&= \beta_t - \beta_{t+1}
\end{aligned} \tag{36}
$$

we can simplify Equation (35) to

$$
\begin{aligned}
y_{t+1} &= y_t \frac{\beta_{t+1}}{\beta_t} + \frac{\beta_t - \beta_{t+1}}{\beta_t} \bar{\epsilon} = \bar{\epsilon} + y_t \frac{\beta_{t+1}}{\beta_t} - \frac{\beta_{t+1}}{\beta_t} \bar{\epsilon}, \\
&= \bar{\epsilon} + \frac{\beta_{t+1}}{\beta_t} (y_t - \bar{\epsilon}).
\end{aligned} \tag{37}
$$

This last form is exactly variant-(b) of IADB (see Table 1). We confirm this experimentally in Figure 16.
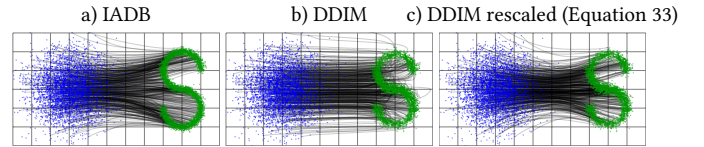

Fig. 16. We trained an MLP with 5 hidden layers of 64 filters to learn D_θ for IADB (a) and the same architecture to learn ϵ_θ for DDIM (b) and (c). For (c), we convert points generated by DDIM using the scaling equation. The trajectories of the samples for IADB (a) and DDIM rescaled (c) match.